Special Issue: Vesuvius monitoring and knowledge

P-wave velocity and density structure beneath Mt. Vesuvius: a magma body in the upper edifice?

Paolo Capuano[1,*], Guido Russo[2], Roberto Scarpa[1]

[1] *Università di Salerno, Dipartimento di Fisica "E. R. Caianiello", Fisciano (Salerno), Italy*

[2] *Università di Napoli "Federico II", Dipartimento di Fisica, Naples, Italy*

Article history
Received September 25, 2012; accepted June 10, 2013.
Subject classification:
Volcanic risk, Tomography and anisotropy, Gravity anomalies, Mt.Vesuvius, Seismic tomography, Gravity inversion.

ABSTRACT

A high-resolution image of the compressional wave velocity and density structure in the shallow edifice of Mount Vesuvius has been derived from simultaneous inversion of travel times and hypocentral parameters of local earthquakes and from gravity inversion. The robustness of the tomography solution has been improved by adding to the earthquake data a set of land based shots, used for constraining the travel time residuals. The results give a high resolution image of the P-wave velocity structure with details down to 300-500 m. The relocated local seismicity appears to extend down to 5 km depth below the central crater, distributed into two clusters, and separated by an anomalously high Vp region positioned at around 1 km depth. A zone with high Vp/Vs ratio in the upper layers is interpreted as produced by the presence of intense fluid circulation alternatively to the interpretation in terms of a small magma chamber inferred by petrologic studies. In this shallower zone the seismicity has the minimum energy, whilst most of the high-energy quakes (up to Magnitude 3.6) occur in the cluster located at greater depth. The seismicity appears to be located along almost vertical cracks, delimited by a high velocity body located along past intrusive body, corresponding to remnants of Mt. Somma. In this framework a gravity data inversion has been performed to study the shallower part of the volcano. Gravity data have been inverted using a method suitable for the application to scattered data in presence of relevant topography based on a discretization of the investigated medium performed by establishing an approximation of the topography by a triangular mesh. The tomography results, the retrieved density distribution, and the pattern of relocated seismicity exclude the presence of significant shallow magma reservoirs close to the central conduit. These should be located at depth higher than that of the base of the hypocenter volume, as evidenced by previous studies.

1. Introduction

Since the last 1944 eruption Mt. Vesuvius is in a quiescent stage. An increase of scientific interest for this volcano dates back in 1981 [Sheridan et al. 1981] when the detailed analysis of pumice flows and other pyroclastic products clearly showed the sequences, in the last 19,000 years, of 5 plinian eruptions and a larger number of subplinian events, the last of which occurred in 472 and 1631 A.D. After this last eruption the activity has been almost continuous, and divided in 18 Strombolian cycles characterized by effusive and moderately explosive eruptions. The last event occurred in 1944. Since 1944 this volcano shows only fumarolic and low level of seismic activity, with the absence of ground uplift episodes. In the last decade of 20th century, a small increase of the magnitude of the largest earthquakes, some felt by population, has been reported [Bianco et al. 1999, Zollo et al. 2002, Del Pezzo et al. 2003]. Volcanological models of Plinian eruptions have been developed through continuous magma filling from a reservoir located in the shallow crust at 3-6 km depth [Rosi et al. 1987, Civetta and Santacroce 1992]. Mount Vesuvius has been the object, in the last decades, of extensive geophysical and volcanological studies [Gasparini et al. 1998]. In particular, seismic tomography has been performed with the objective of improving the knowledge of the deep structure and extent of magma reservoir below Mt. Vesuvius; this knowledge is essential to provide more realistic simulation models of the eruptive activity and is the base for a precise identification of possible precursors of future eruptions. Dense seismic recorded land shots and marine airgun signals generated during experiments carried out in 1994, 1996 and 1997 have been analyzed with the main purpose of defining the geological structures beneath Mt. Vesuvius [Zollo et al. 1996, Auger et al. 2001]. These results revealed the presence of a large low P-wave velocity body, looking like to a very large sill located at an average depth around 8 km, extending from Mt. Vesuvius toward East and in the direction of the nearby volcanic center of Campi Flegrei, covering a surface larger than 300 km^2. These results show a quite ho-

mogeneous geological structure in the upper 5 km below the topographical surface of Mt. Vesuvius, having an alternance of high and low velocity layers for P-waves, which has been mostly linked to the morphology of the limestone basement on which the whole region lays [Principe et al. 1987]. Consequently, the small-scale details of the shallow structure obtained in these previous studies can be considered as unfocused, indicating the necessity to use higher resolution tomography methods.

The deployment of dense seismic arrays is a diffused technique for studying details of the seismic sources in relation to volcanic activity, other than a method for understanding the velocity structure beneath these regions and for improving volcano monitoring techniques [see, e.g., Ferrazzini et al. 1991, Goldstein and Chouet 1994, Metaxian et al. 1997, Chouet et al. 1998].

During the seismic tomography experiments carried out on Mt. Vesuvius in 1994 and in 1996 we get the opportunity to install small aperture seismic arrays along the crater rim and on its southern flanks. Later on, in 1997-1998, for a period lasting several months, another small array has been deployed along the southern flanks of this volcano, at an intermediate altitude (about 600 m.)

The main scientific objectives were: a) to record the seismic waveforms from artificial explosions, with dense space and time sampling of the seismic signal, to image the velocity structure and the distribution of the strong elastic scatterers in the upper layers under the central crater, with a very high resolution; b) to study the response of different sites on the flanks of Mt. Vesuvius, in order to optimize the installation of a permanent small aperture array for volcano monitoring. In the zone of Mt. Vesuvius the presence of a highly fractured material and topographical irregularities generate a high degree of heterogeneity of seismic velocities increasing the signal-generated noise that strongly affects the seismic signal. Moreover a strong cultural noise, generated by the human activity in one of the most densely inhabited area of Italy and by the presence of the sea, further reduce any capacity of detecting small seismic signals related to a possible reawakening of volcanic activity.

Results obtained till now have been published in the papers by De Luca et al. [1997], La Rocca et al. [2001] and by Scarpa et al. [2002], proposing a high-resolution seismic tomography image. The aim of the present paper is to critically review these results and to furnish further details on the data and resolution power of the results obtained by Scarpa et al. [2002], focusing on the problem of detecting the presence of a shallow magmatic reservoir and the interpretation of the present seismicity of this volcano. These results have been improved by the inversion of gravity data that was able to detect the density structure of the shallower part of the volcano edifice above the limestone basement, adding constraints to the structural model.

2. Instruments and array deployment

During the 2D seismic tomography experiment performed in the period 4-6 May 1994 [Zollo et al. 1996], two dense arrays of short period seismographs were installed by teams of the Physics Departments of L'Aquila and Salerno University along the crater rim of Vesuvius (Figure 1a). The first array, maintained by the Salerno group, consisted of 15 vertical seismographs, natural frequency 4.5 Hz, connected by cables to a 12 bits data acquisition system controlled by a PC-IASPEI data acquisition system [Lee and Dodge 1992]. The second array, developed by the group from L'Aquila University, was formed by 25 vertical and 2 horizontal seismographs, with natural frequency 4.5 Hz, located next to the previous array. This array consisted of a light portable unit, with transducers linked by cables to a data acquisition system having a resolution of 16 bits. Both equipments were synchronized by the same time signal, the coded DCF 77, provided by two radio receivers, and recorded on a separate channel. The spacing between the seismometers for both arrays was 30 m and close to the center of the second array additional 8 seismometers, deployed according to an ellipsoidal shape, were installed. The total aperture for both arrays has been about 1 km.

During the 3D TomoVes program held in June 1996 the group from L'Aquila University deployed a small aperture seismic array composed by 21 short period three component and 15 short period vertical component, along the South flanks of Mt. Vesuvius [La Rocca et al. 2001]. The same data acquisition system and transducer type of that used in the 1994 experiment were used, covering a 200 m $\times$ 70 m region, with the stations positioned along six radial lines from the center of one long edge.

In November 1997 a seismic array formed by short period seismometers was installed by University of Granada, University of Salerno, and Vesuvius Observatory on the SW flank of Mt. Vesuvius with the main aim to test novel array techniques for an improved volcano monitoring (VESARRAY experiment, see also the Open File Report on line, at www.ov.ingv.it). The location site is inside the national park, at 1.5 km distance from the crater and is characterized by relatively smooth topography, with 10° as average slope. The size of this array, having an almost circular geometry, is about 500 m in diameter. This array was formed by 18

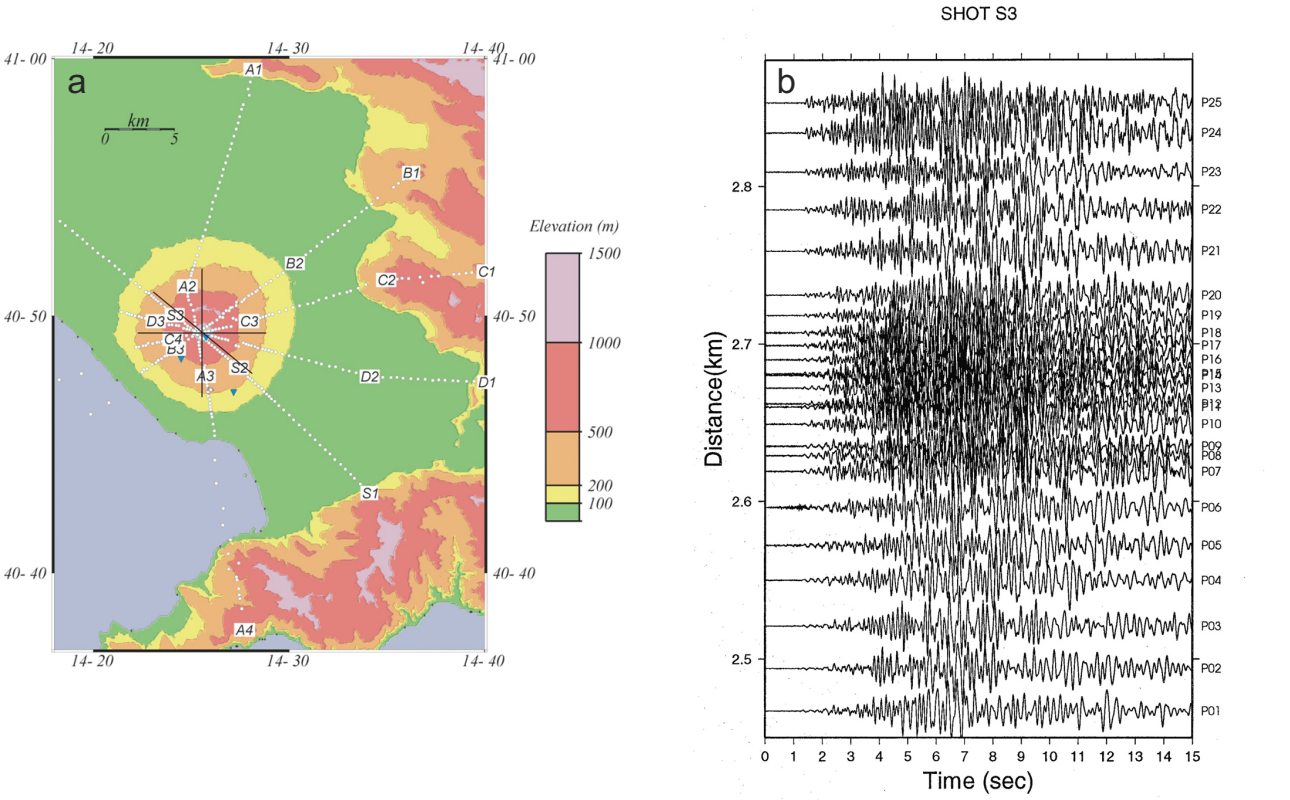

Figure 1. (a) Topographic map of the Somma-Vesuvius region showing the Tomoves 1994 (line S) and 1996 (lines A-D) seismic profile stations (circle) and shotpoints (A1, A2, etc.). Closed triangle correspond to seismic array deployments and black lines correspond to the trace of N-S, E-W and NE-SW seismic sections shown in Figure 4; (b) Example of seismic recording of the shot S3 during the 1994 TOMOVES experiment (after De Luca et al. [1997]).

vertical geophones and 1 three-component seismometer Mark L15B. The natural frequency (4.5 Hz) of the seismometers was electronically extended to 1 Hz. The array was composed by three subarrays, controlled by three data acquisition systems. Each data logger is formed by a 16 bits A/D converter, an anti-aliasing filter and a GPS control circuit connected to a GPS antenna for absolute timing. Signals were sampled at 200 Hz. A detailed description of the instruments is reported in Ibanez et al. [2000] and a description of the array site and configuration by Saccorotti et al. [2001]. During the 7 months of array operation, local seismicity, regional earthquakes and seismic noise were recorded and organized in a data base. In the course of the present paper we well refer to Deployment 1 (D1), Deployment 2 (D2) and Deployment 3 (D3) to the experiments carried out respectively in the 2-D Tomography, 3-D tomography and VESARRAY (see Figure 1a).

2.1. Seismic velocity and reflecting interfaces

The array recordings of the three shots fired for the 1994 experiment (D1) reveal at a first visual analysis a low degree of spatial coherence, a low degree of coherence in the waveforms of late arrivals and a complex particle motion pattern (Figure 1b). This observation is consistent with the presence of strong scattering and diffraction effects. These are possibly due to the strong heterogeneity affecting the geological structure on which the antenna was installed and/or to an effect of resonance from upper layers, modulated by the irregular topography around Vesuvius crater.

In order to quantify this observation data processing was carried out for records from shots S2 and S3 (Figure 1a), closest to the volcano, disregarding the data from the array 1, for their amplitude saturation due to the relatively lower dynamic range. We considered consequently the array formed by 25 vertical receivers, having a linear extension of about 450 m.

The data have been analyzed through the software Seismic Unix [Cohen and Stockwell 1994]. The seismic records have been corrected for the offset, by using the origin times of the shots and a time window of 30 s. Records have been also corrected for the elevation by shifting the travel-time of each station by a quantity $dt=dz/V$, where dz is the difference between the altitude of the stations and those of the shots, and $V=2.3\pm0.25$ km/s deduced from the work by Zollo et al. [1996]. Records have been also filtered in the band 2-15 Hz and their amplitudes normalized using the procedure Automatic Gain Control (AGC) with 2 s time windows for the shot S2 and 3 s for the shot S3. Synthetic seismograms have been also generated in order to test the delay expected with simple models. For instance, by using a schematic model to represent condi-

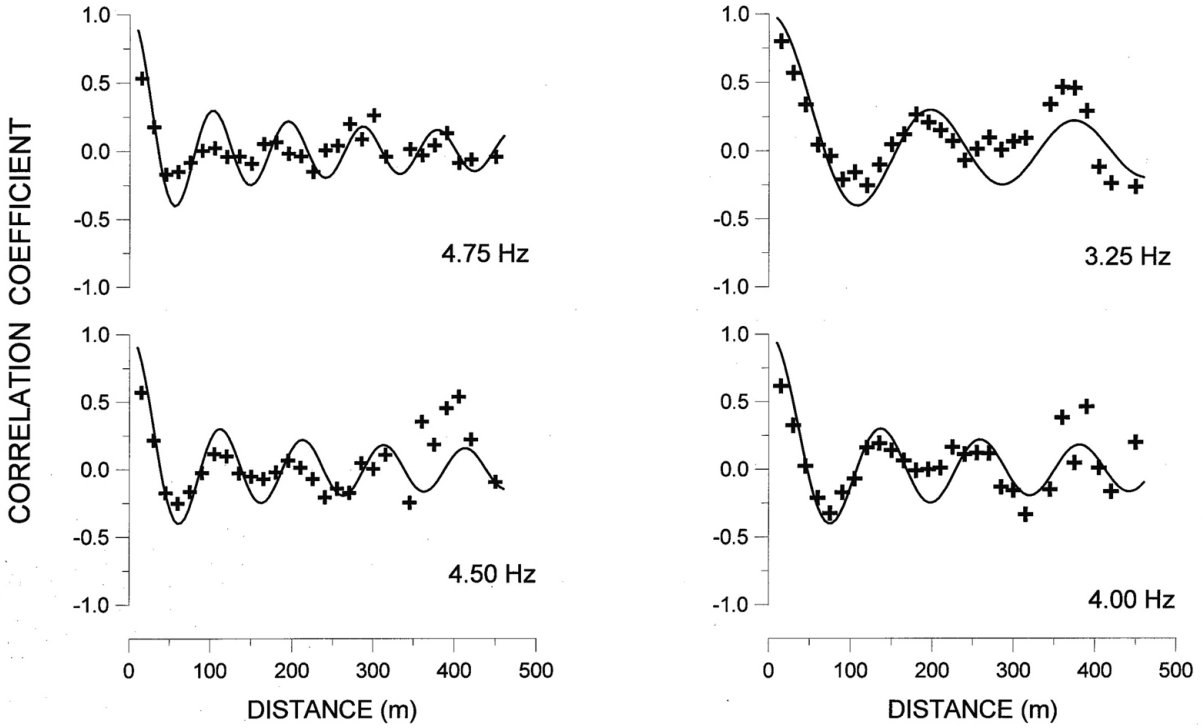

Figure 2. Examples of comparison between theoretical and experimental correlation curves for the vertical component at 3.25 Hz, 4.00 Hz, 4.50 Hz and 4.75 Hz.

tions for the S3 shots: offset of the array 2.5 km and relative distance 30 m, flat surface of reflection located at 2.0 km depth and constant P-wave velocity V=2.3 km/s, the expected arrival time of the first reflection is 2.0 s after the origin time. The procedure of Constant-Velocity stacking applied to synthetic seismograms allows to obtain the true velocity and the depth of the reflector. Using the same procedure to data from shots S3 in a velocity range 1 km/s < Vs < 8 km/s, with 500 m/s steps in a window 0-3 s, and lately in the range 1 km/s < Vs < 4 km/s with steps dv=200 m/s, it can be observed a flattening in correspondence of the velocity V=1.8±0.2 km/s and a value of the two-way time t_0=1.8±0.1 s, from which it can be deduced, for shot S3, a depth of the reflector h=1.6±0.2 km. For the shot S2 in the same time window it is obtained V=2.2±0.2 km/s and t_0=2.1±0.1 s and consequently a reflector depth h=2.3±0.2 km. By considering the model simplifications, basically flat reflection surface and constant velocity averaged through the ray path, the depths resulting in the two time windows can be considered as consistent. The arrival of the first reflection occurs 1.8 s later from the shot S3 and the arrival at 4.2 s can be interpreted as a multiple reflection. The same occurs for the shot S2. The arrival time of the reflected phase for S2 and S3 is consistent with the simulations performed with the best fit model derived from the interpretation of the whole seismic profile discussed by Zollo et al. [1996]. The result obtained from these last authors suggests that the horizon K (limestone) is located deeper for shot S2 than for S3. The small aperture array installed along the crater rim confirms this relevant result.

3. Velocity and density structure

3.1. Shallow velocity models

The SPatial Autocorrelation Method (SPAM, Aki [1957]) has been used to infer the shallow velocity structure by using microtremor records. This method is based on the estimate of the azimuthal average of spatial correlation coefficients between pairs of signals, computed in narrow frequency bands, that has a theoretical behavior linked to the zero order Bessel function. This is true for vertical component records and wavetrains formed by Rayleigh waves [Aki 1957]. Chouet [1996] extended this method to the horizontal components in order to infer dispersion curves of Rayleigh and Love waves, linked to combination of Bessel functions derived from correlation coefficients of radial and transversal components. The data collected at Mt.Vesuvius are basically from vertical components and contains some minutes of microtremor records, other than the artificial explosions. The signals within a time window 6'20" have been filtered in 37 very narrow (0.5 Hz) bands in the frequency interval 1-10 Hz. Cross-correlation coefficients and their azimuthal averages, over 300 distance ranges in the interval 0-500 m, have been computed for each central frequency of these bands.

The correlation-frequency curves for several sets of distances have been then calculated and fitted with Bessel functions (Figure 2). Since Bessel functions have

terms depending on the velocity of surface waves, dispersion curves have been determined. By using trial and error inversion techniques [Haskell 1953, Horike 1985] a best fit velocity model has been derived (Figure 3). This result is well consistent, in spite of the low resolution for the deeper layer, with measurements made during the tomography experiments and provides a good constraint for high resolution tomography of the summit crater of Mt. Vesuvius.

For the 1997-98 experiment eighteen 120-sec long time windows recorded by the vertical component sensors at different hours of the day have been analyzed. Being the instruments response constant in the 1-50 Hz frequency range for all the sensors, the instrument correction has not been performed. The hypothesis of a stochastic and stationary wave field imposed by the Aki's method, requires long time windows to determine the average characteristics of the seismic noise. The length of the recorded signals has been checked for performing the statistical analysis. In fact the correlation coefficients computed on increasing time windows of the filtered signals were stable even for 80 sec long time windows.

The recorded signals were filtered in the 1.5-10 Hz frequency range, with bandwidth 0.5 Hz, at central frequencies spaced 0.25 Hz. For each central frequency of these bands, correlation coefficients over 170 distance ranges in the interval 40-450 m have been computed for each pair of stations. The curves superimposed on the data in Figure 3 were derived by fitting the experimental correlation coefficients to the Bessel function J_0. In these fits the arguments of the Bessel function is computed on the basis of a dispersive trend expressed by the relation:

$$C_R(f) = Af^{-b}$$

where $C_R(f)$ is the Rayleigh wave velocity, f is the frequency, and A and b are constants. An example of dispersive curves as expected by the previous equation is shown in Figure 3, for one record at 20h59m, whose coefficients have been fixed by least square method. The error on the velocity values represents the ranges of values on which the minimization is performed. The results obtained on eighteen different time-windows are in good agreement, giving a low standard deviation (less than 0.1%) on the velocity values.

3.2. 3-D seismic tomography

The detailed knowledge of velocity in the upper 300–500 m allows to optimally constrain the finite difference ray-tracing and favor the application of tomographic methods based on the simultaneous, linearized inversion of 3-D velocity structure and earthquake locations from travel time data. The results described above were consequently used for the application of the technique described by Benz et al. [1996] to obtain a detailed tomography of the upper 3-4 km beneath Mt. Vesuvius. This method has been used on several volcanoes in the world, such as Redoubt, Kilauea and Etna [Benz et al. 1996, Okubo et al. 1997, Villasenor et al. 1998], to obtain high resolution images at a scale of few hundred meters, in the region covered by rays connecting hypocenters to stations.

Data used in the present study have been collected from the seismic monitoring network of Osservatorio Vesuviano in the period 1987-2001, which includes a period of relatively higher seismicity as compared to the last decade. Accurate readings of P- and S-arrivals have been obtained from a set of 600 microearthquakes selected from 2139 events recorded from a minimum number of 7 to 19 temporary and permanent seismic stations resulting in a set of 8,600 P-wave and 1,900 S-wave readings. Theoretical travel times are calculated using a finite-difference technique. We selected a region 9×9 km^2 centered around the main crater and extending down to 5 km depth, corresponding to the most intense ray coverage. This volume has been parametrized using uniform $0.3 \times 0.3 \times 0.3$ km^3 constant velocity cells. Finer grids down to $0.15 \times 0.15 \times 0.15$ km^3 are used for travel time calculations. Tomographic inversion runs provided 70-80% reduction in the RMS arrival times after 10 iterations from a starting RMS value of 0.35 s, giving travel time residuals comparable with phase reading errors (total RMS value is 0.15 s).

Several tests have been performed to determine the effects of initial reference velocity model, using different 1-D models derived from inversion of shots and

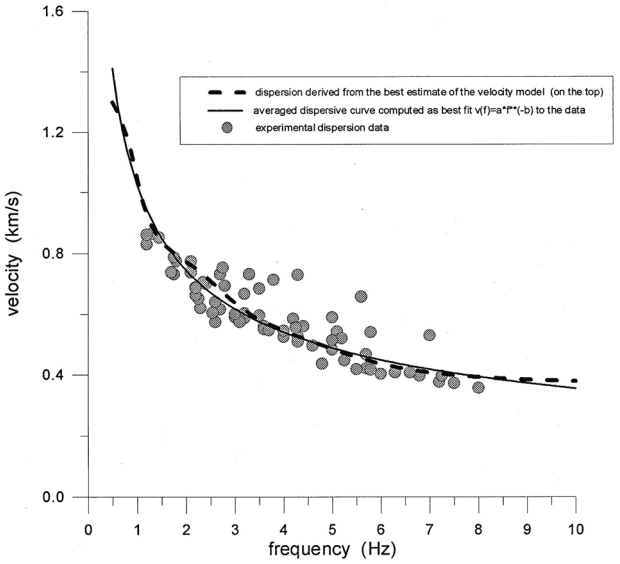

Figure 3. Comparison between dispersion curves observed and modeled for Rayleigh waves.

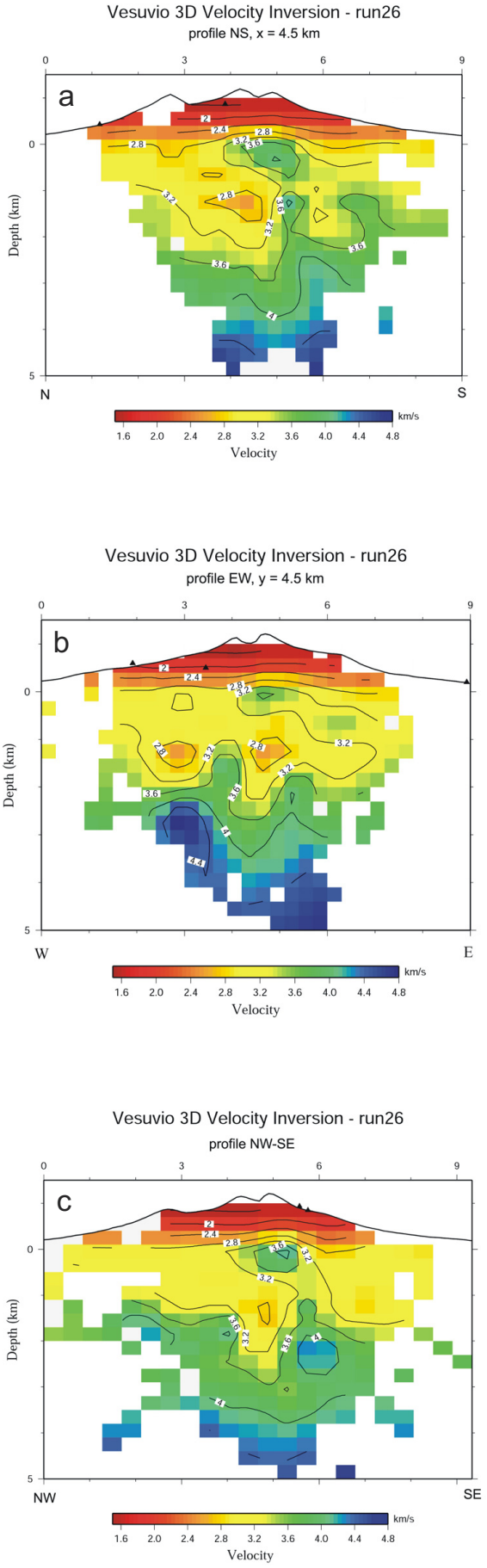

Figure 4. (a) NS (b) EW and (c) NW-SE cross sections of the P-wave velocity structure. Only well resolved blocks (>10 rays) are represented.

earthquake data. The resolution analysis is done empirically by mapping the ray-path coverage and performing synthetic checkerboard reconstruction tests, by using the source receiver geometry of our data set. Different grids, varying from cells having 0.3 to 0.8 km size have been also tested. In the plots of Figure 4 and Figure 5, representative of one of the most stable velocity models, only cells having well resolved velocity anomalies, corresponding to a number of rays larger than 10 for each block, are plotted.

We found evidence of strong vertical and lateral P-wave velocity variations in the upper 5 km, i.e. the region spanned by earthquake activity (Figure 6). The relocated hypocenters are splitted into two clusters and concentrated in a small cylinder, extending laterally about 1 km and vertically from surface down to a depth of 5 km. Two high velocity bodies are clearly visible: the first is located below the craters and extended from the sea level to a depth of 1 km, just above a low velocity region, extended about 2 km in depth. The second is located in the South direction, possibly indicating a high concentration of dykes which is in connection at surface with the larger distribution of lateral eruptive vents present in this sector. At a depth varying from 1.5 to 2.5 km below the volcano, it is possible to delineate a high velocity layer which well fits the top of the limestone basement already evidenced by gravimetric and seismic reflection studies and from data of a deep drilling borehole [Cassano and La Torre 1987, Di Maio et al. 1997]. As the present data set does not allow to perform a complete tomographic inversion of S-wave arrivals, due to the small number of S readings available at the 3-component seismic stations, we computed the Vp/Vs ratio in a multilayered 1-D model using a selected set of P and S-phase readings. The result shows that materials beneath Mt. Vesuvius seismic stations are characterized by high values of Vp/Vs (>1.8) ratio, with an increase to the value of 2.0 in the depth range 0.5-1.5 km b.s.l. These values are consistent with V_S values inferred from the surface wave dispersion analysis performed by Natale et al. [2005] and with the inversion performed by De Natale et al. [2004]. We are well aware however that the available data set cannot provide a reliable 3D inversion of Vp/Vs, due to the relatively low number and quality of S first arrivals.

3.3. Inversion of gravity data

Gravity measurements on land and off shore of Vesuvius area and its surroundings have been collected. Data come from several surveys performed by different institutions. We collected measurements on land by Tribalto and Maino [1962], Cassano and La Torre [1987] and Servizio Geologico d'Italia (unpublished data), and

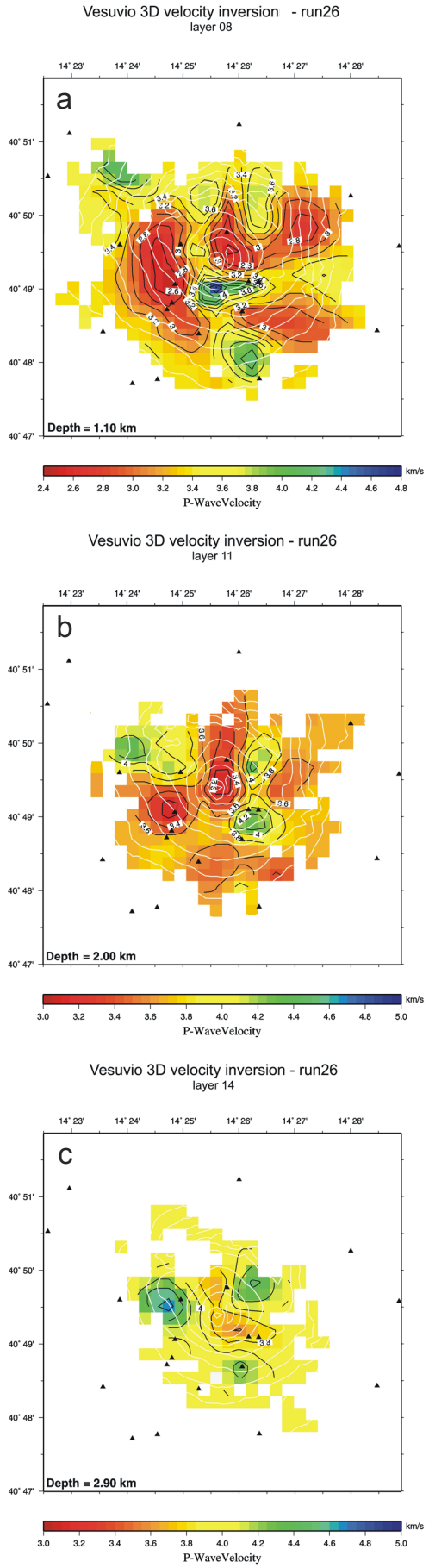

Figure 5. Velocity contours at (a) 1.1 km depth (b) 2.0 km depth and (c) 2.9 km depth. Black triangles indicate seismic stations. Only well resolved blocks are represented.

offshore in the Gulf of Naples by Berrino et al. [1998]. To obtain a better data coverage in the southern part of the investigated region, gravity measurements have been added using the Gravity Map of Italy [Carrozzo et al. 1981]. These data have been integrated with measurements collected at the end of the '90s in the summit area of Mt. Vesuvius [Bruno et al. 1997]. Gravity measurements were made homogeneous by referring them to the IGSN71 network. Then, we revised data to eliminate inconsistencies due to their different origin and to clearly erroneous measurements. At the end of this process, our data set consists of 777 gravity measurements covering an area of 22×20 km^2 centered on Mt. Vesuvius. We computed free air correction with reference to the GRS80 ellipsoid. To compute the terrain correction we extracted almost 6000 points from a DEM covering an area of 80×60 km^2 centered on Mt. Vesuvius, of which more than 400 in the Mt. Vesuvius summit area. We built a triangular mesh connecting all the points approximating the shape of the topography of the area. Below each triangle we built a triangular prism, the attraction of which can be computed analytically using the method outlined by Okabe [1979]. We chose for the densities of the prisms the value 2400 and 2200 kg/m^3. The first value was assigned to the prisms belonging to the mountains surrounding Mt. Vesuvius, while the second was assigned to the prisms belonging to the flat portion of the Campania plain, and to the volcanic edifice [Berrino and Camacho 2008]. To subtract the effect of sea water we integrated the set of offshore measurements with points extracted from a larger scale bathymetric map, thus obtaining a set of 3200 points distributed over an area of about 10400 km^2, large enough to consider border effect negligible. Using again an approximation of sea floor shape by a triangular mesh we computed the effect of sea water using a density of 1030 kg m^{-3} [Stabile et al. 2007]. We show the computed Bouguer anomaly map in Figure 7a. Out of the central part, where the gravity field is dominated by the effect of the volcanic structure, at the borders the field is well correlated with the shape of the limestone platform [Lomax et al. 2001, Judenherc and Zollo 2004]. To remove this regional effect, we represented the regional field as a eight-nodes shape function, and optimized the value at the nodes using a downhill simplex minimizing the L_1 norm of the residual field obtaining an average misfit of 2.7 mGal. We show the resulting field in Figure 7b. We see some still uncompensated effects of the basement to the South, to the East, where the it outcrops nearby the border of the model, and at the West, where the basement dips downward. Two minima are present to the Southeast (Pompei depression) and to the Northwest (Acerra de-

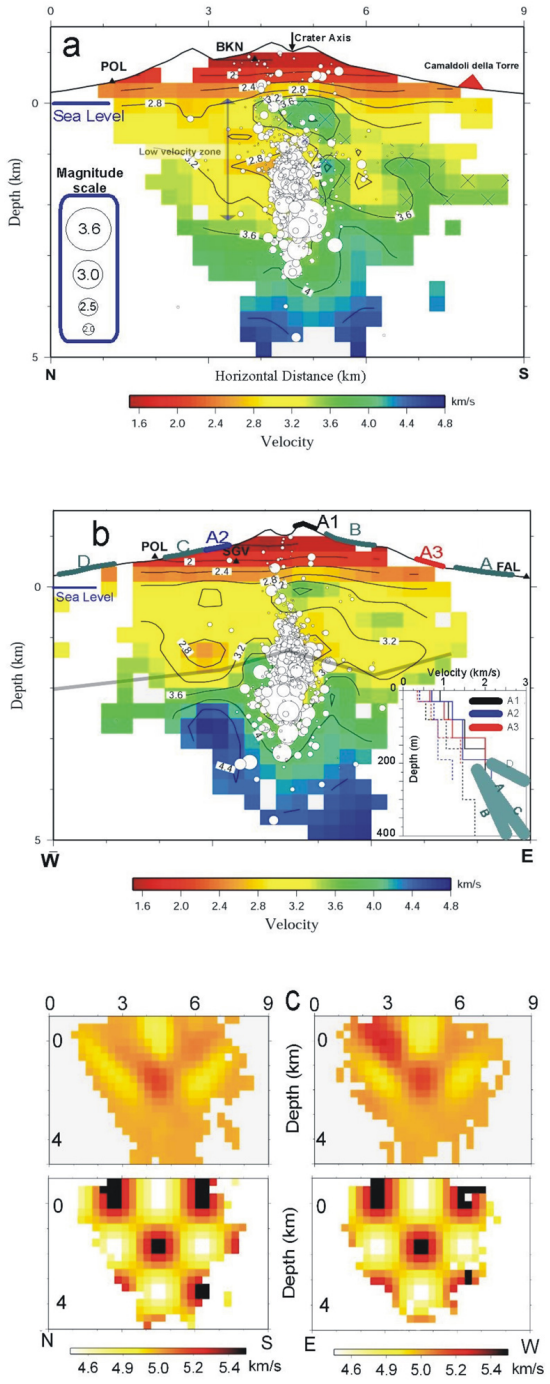

Figure 6. (a) NS and (b) EW cross sections of the P-wave velocity structure. White circles show the relocated hypocenters having size proportional to magnitude. The shallow high-velocity bodies located beneath and Southward to the crater, are evidenced with a semi-transparent zone filled by blue crosses. The low velocity layer toward N is linked to the deepening of the limestone basement. Camaldoli della Torre is the main lateral cone of the highly fractured zone extending Southward the crater. The grey-transparent line is the top of the carbonates, drawn from Figure 2 by Lomax et al. [2001]. The inset in (b) shows P- and S-wave velocity-depth functions (continuous and dashed lines respectively) derived at the three sites around Mount Vesuvius (colors are related to A-1, A-2 and A-3 arrays shown in Figure 1) from dispersion characteristics of background seismic noise. The heavy bold green lines marked with A,B,C and D are redrawn from Figure 6 of De Matteis et al. [1997]. (c) Checkerboard resolution test carried out using a 300 m square grid is represented in the same sections used for (a) and (b) (after Scarpa et al. [2002]).

pression) that are related to the morphology of the basement [Cella et al. 2007]. As to the volcano, we see two relative maxima just North, corresponding to Mt. Somma, and South of the crater. A relative minimum located exactly over the crater separates the two maxima.

To invert the data, we considered again the 777 on land and off shore data points to which we added 707 points, more than 400 in the summit area of the volcano, to improve the approximation of the shape of the topography by means of a triangular mesh. Under each triangle we built a sequence of triangular prisms. Each prism generates a known gravity attraction, so they can be grouped together to achieve a quasi-regular parametrization and a layered structure as shown in Figure 8a, left part. On a planar scale, we grouped triangles to have quasi regular-blocks of 0.815×0.8 km^2.

To solve the linear discrete inverse problem

$$A\mathbf{x} = \mathbf{b}$$

where A is the matrix of the gravity attraction generated by the blocks of our model, assumed having unit density, at data points, $\mathbf{x}$ is the vector of the unknown densities of the blocks, and $\mathbf{b}$ is the data vector, we used the Tichonov regularization theory imposing on $\mathbf{x}$ the constraint of minimum norm [Zhdanov 2002]. This corresponds to minimize the functional

$$P = ||\mathbf{Ax-b}||^2 + \alpha ||\mathbf{Wx}||^2$$

where $\mathbf{W}$ is a constant diagonal matrix representing the sensitivity of data to changes of $\mathbf{x}$, and α is a parameter that has to be evaluated according to the method of Hansen [1992] and is linked to the minimum misfit required from the inversion.

The resulting model has an R.M.S. of 0.7 mGal (Figure 8b) The resolution is shown in the right part of Figure 8b. The figure shows that the model is resolved down to 2.5-3 km depth.

Horizontal sections through the 3-D gravity model, at different depth, between 800 m elevation and 5000 m b.s.l., are reported in Figure 9, together with the elevation contour line (upper left in the figure). The gravity sections, taking into account for the lateral resolution of the gravity model (800 m) evidence that above 400 m a.s.l., the density is rather heterogeneous due to the presence of different lithologies as lava and pyroclastic flows, but a maximum in density starts to be evident in correspondence to the Mt. Somma. The crater area shows a lower density. Between 400 and 0 m a.s.l. a second density maximum is evident south of the crater. This maximum is consistent with that shown by the seismic tomography (see Figures 4 and 6). The first

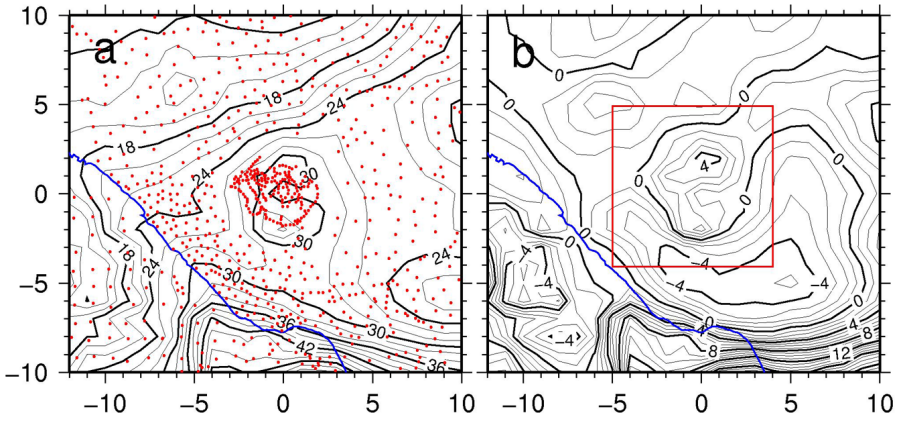

Figure 7. (a) Bouguer anomaly map contoured at 2 mGal step together with the location of the gravity stations (red points). Blue line represents the coastline; (b) Residual gravity field after the regional trend removal (see text). For comparison, red box indicates the area covered by the seismic tomography inversion.

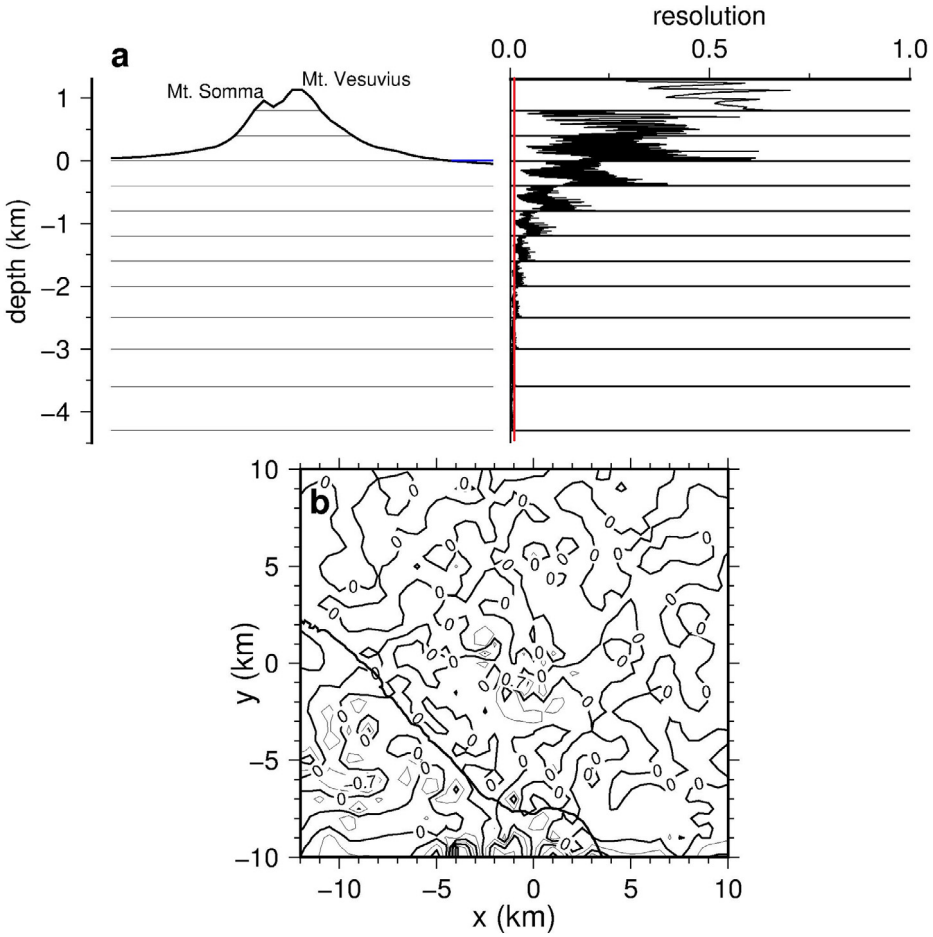

Figure 8. (a) left: sketch of the basic structure (layer) used to parameterize the density distribution; right: resolution for each layer of the model. As a reference, a (red) line corresponding to a 3 percent of the maximum value of resolution has been plotted; (b) gravity misfit of the computed anomaly with respect to the observed field.

maximum, instead, is not evident in the seismic sections, but it is located, differently from gravity data, at the border of the area covered by seismic rays and is consistent with the results of De Matteis et al. [1997] that evidenced the presence of a high velocity body in correspondence of Mt. Somma. The two density maxima show deep roots at least up to 2 km b.s.l. The central lesser density zone is evident up to about 1 km b.s.l. Below this depth we do not see any clearly defined high velocity body as shown in seismic sections, but we have to remark that the dimension of that body is of the same order of magnitude of the cell of the inversion, so the resolution may not be sufficient to single out this anomaly. Below 1 km depth the roots of the two maxima seem to be separated by a less dense zone in correspondence to the crater.

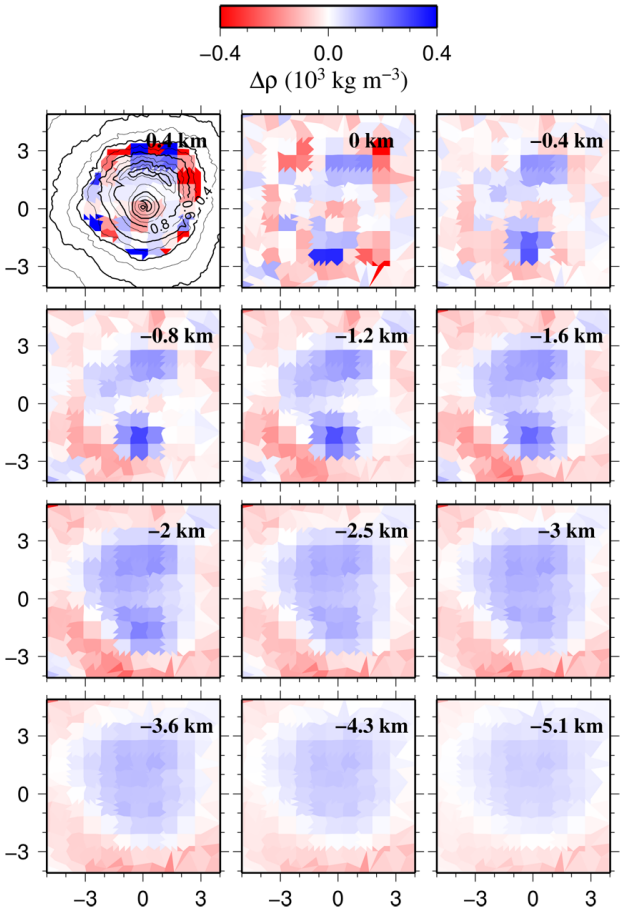

Figure 9. Horizontal sections through the 3-D gravity model, at different depth (the depth indicates in the upper right of each box is referred to the bottom of each layer. In the upper left box the elevation contour lines are also shown. The dimension of each box corresponds to the area covered by the seismic tomography as illustrated in Figure 7b.

4. Discussion

A number of results about Mt. Vesuvius tomography, all aimed at refining the details of the shallow geological structures evidenced by TOMOVES experiments, suffer from low resolution in the rock volume located beneath the crater area, mainly due to the quantity and quality of data used. These papers [De Natale et al. 1998, Lomax et al. 2001, Di Stefano and Chiarabba 2002, Tondi and De Franco 2003, De Natale et al. 2004, Piana Agostinetti and Chiarabba 2008] use only the first arrivals from shots and make a quite limited use of earthquake data. Notwithstanding the above restrictions, these studies have clearly imaged the structure of the Mesozoic limestone basement underlying the volcano edifice and its surroundings, showing the presence of depressions around Vesuvius and indicating the presence of a high velocity body below the volcano. The resolution of these methods are in the range 1-3 km, depending on the wavelength and the ray illumination.

The use in the present study of a higher number of local earthquakes with the addition of constraints from land shots has made possible to delineate a high resolution image within the upper 5 km beneath craters, showing new details of the upper volcanic edifice. In addition, the gross features resulting from our inversion correspond to those evidenced by other studies, confirming the likelihood of the present results. Interesting is also the result about the relocation of the seismicity, which shows that the main seismogenic area is located in a depth range from surface to 5 km, within a small plume located beneath the central crater. In particular the relocated microearthquakes (all volcano-tectonic, VT, events) are not homogeneously distributed in depth but are splitted into two main clusters: the shallower one is located in the upper volcanic edifice and the deeper one, showing the largest number and energy of events, is located in the depth range 2-4 km b.s.l. The two clusters are separated by a high P-wave velocity region having a volume of less than 1 km^3. The deeper cluster occurs within a graben-like structure, limited in the southern side by a high velocity/density body. The higher detail reached by the present observation, unlike other interpretations [see e.g. Tondi and De Franco 2003] indicate that the seismicity does not occur entirely within an intrusive, or horst-like, body. The high velocity body that borders the fractured region, as resulting from our revised earthquake locations, is slightly displaced from the hypocenter volume, and it may correspond to an intrusive body possibly representing the remnant and submerged part of the rim of Somma volcano. Feature like this one have been observed also at some other volcanoes such as Etna [Villasenor et al. 1998, Patanè et al. 2002].

As a consequence of the above considerations, in our view the present seismicity occurs along faults located beneath the most recent volcano plumbing system and a remnant of an older intrusive body. Moreover it is noteworthy that the two seismicity clusters are separated by the anomalous Vp/Vs zone as reported by Scarpa et al. [2002]. This last zone is not wider than 1 km^3 and shows an evident lack of seismicity. There are two possible hypotheses explaining its nature: a) it is a magma pocket residual, and b) it is a hydrothermally altered zone. The hypothesis b) is well supported by the well known presence of acquifers at the same depth at which the Vp/Vs anomaly is observed [Ventura and Vilardo 1999]. We favour the hypothesis b) and base all our considerations on the seismological observation, in the framework of the following conceptual model. It is likely that after the last 1944 eruption the conduits have been emptied. This is consistent with the presence of volcano-tectonic earthquakes (generated by brittle fractures) just in correspondence of the eruptive cone, to a depth of 4 km b.s.l. and with the absence of any LP (long period) or tremor event [Del Pezzo et al. 2003], generated by the effect of fluid movements into cracks in presence of a hot rock.

Consequently, it is hard to image why an isolated magma pocket should be already present only at low depth, giving no signs of its interaction with surrounding fluids. Moreover, the Vp/Vs anomaly is located at the base of a low density zone that can be interpreted as a fractured zone in which fluid circulation can occur.

The cause of occurrence of the shallower cluster of VT earthquakes can be instead well explained by the sole presence of aquifers, causing a high circulation of fluids. The aquifers are likely an important factor controlling the time distribution of seismicity [Ventura and Vilardo 1999, Saccorotti et al. 2002]. This hypothesis is consistent with the observed Vp/Vs pattern, which can be interpreted as due to presence of rocks with high porosity and permeability [O'Connel and Budianski 1977], similarly to that observed in the nearby Campi Flegrei volcanic area [Aster et al. 1992] and with the density contrasts evidenced in this study.

At the light of all the above considerations the seismological data confirm that the present magma should be located below the base of hypocenter volume, i.e. at least below 5 km depth, as hypothesized by Piana Agostinetti and Chiarabba [2008] on the basis of their inversion of Vp and Vs arrivals of local earthquakes.

The overall results reviewed in the present paper evidence also that the upper structure of Mt. Vesuvius is characterized by a quite heterogeneous environment. Scatterers are highly concentrated around the volcanic edifice, in agreement with the hypothesis that the topographical irregularities play a major role in the generation of high frequency scattering phenomena. The vertical variations of both seismicity and velocity properties suggest a strong permeability of rocks and high circulation of fluids in a depth range 0.5-1.5 km b.s.l., just above the limestone basement which is also well revealed by our study. The presence of a pronounced acquifers below the central crater is in agreement with data from geoelectric and geochemical surveys. This layer has certainly played a major role in the past eruptions causing relevant hydrothermal events during both plinian and subplinian events. The present interpretation may assume some relevance for understanding the mechanism of past and future eruptions and for identifying their possible precursor phenomena. The zone which reveals to be crucial from this point of view is that located at a depth between 5 and 8 km, in the region between the bottom of seismogenic zone and the average depth of top of magma chamber inferred by the results of TOMOVES experiments.

Acknowledgements. This work has been partially supported by grants of MIUR, CNR-GNV, DPC-INGV and UE. Data collected during the TOMOVES experiment have also been used.

References

Aki, K. (1957). Space and time spectra of stationary stochastic waves, with special reference to microtremor, Bull. Earthq. Res. Inst. Tokyo Univ., 25, 415-457.

Aster, R.C., R.P. Meyer, G. De Natale., A. Zollo, M. Martini, E. Del Pezzo, R. Scarpa and G. Iannaccone (1992). Seismic investigation of the Campi Flegrei: a summary and synthesis of results, In: P. Gasparini, R. Scarpa and K. Aki (eds.), Volcanic Seismology, IAVCEI Proceedings in Volcanology, Springer, Berlin, 462-483.

Auger, E., P. Gasparini, J. Virieux and A. Zollo (2001). Seismic evidence of an extended magmatic sill under Mt. Vesuvius, Science, 294, 1510-1512.

Benz, H.M., B.A. Chouet, P.B. Dawson, J.C. Lahr., R.A. Page and J.A. Hole (1996). Three-dimensional P and S wave velocity structure of Redoubt volcano, Alaska, J. Geophys. Res., 101, 8111-8128.

Berrino, G., G. Corrado and U. Riccardi (1998). Sea gravity data in the Gulf of Naples: a contribution to delineating the structural pattern of the Vesuvian area, J. Volcanol. Geoth. Res., 82, 139-150.

Berrino, G., and A.G. Camacho (2008). 3D gravity inversion by growing bodies and shaping layers at Mt. Vesuvius (Southern Italy), Pure Appl. Geophys., 165, 1095-1115.

Bianco, F., M. Castellano, G. Milano, G. Vilardo, F. Ferrucci and S. Gresta (1999). The seismic crises at Mt. Vesuvius during 1996 and 1997, Phys.Chem.Earth, 24, 977-983.

Bruno, P.P.G., E. Carrara, F. Cella, V. Di Fiore, A.S. Dorre, M. Fedi, G. Florio, M. Grimaldi, R. Pagetta, N. Roberti and G. Russo (1997). Indagini gravimetriche, magnetometriche e di sismica a riflessione al Vesuvio; presented at the GNV-CNR Annual Scientific Workshop, Rome.

Carrozzo, M.T., A. Chirenti, D. Luzio, C. Margiotta, T. Quarta and F. Zuani (1981). Carta gravimetrica d'Italia: tecniche automatiche per la sua realizzazione, In: Atti I Convegno GNGTS, CNR, Rome, 131-140.

Cassano, E., and P. La Torre (1987). Geophysics, In: R. Santacroce (ed.), Somma-Vesuvius, Quaderni de "La Ricerca Scientifica", CNR, 114, 175-196.

Cella, F., M. Fedi, G. Florio, M. Grimaldi and A. Rapolla (2007). Shallow structure of Somma-Vesuvius volcano from 3D inversion of gravity data, J. Volcanol. Geoth. Res., 161, 303-317.

Chouet, B.A. (1996). New methods and future trends in seismological volcano monitoring, In: R. Scarpa and R. Tilling (eds.), Monitoring and Mitigation of Volcano Hazards, Springer-Verlag, New York, 23-97.

Chouet, B.A., G. De Luca, G. Milana, P. Dawson, M.

Martini and R. Scarpa (1998). Shallow velocity structure of Stromboli Volcano, Italy, derived from small-aperture array measurements of strombolian tremor, Bull. Seismol. Soc. Am., 88, 653-666.

Civetta, L., and R. Santacroce (1992). Steady-state magma supply in the last 3400 years of Vesuvian activity, Acta Vulcanol., 2, 147-159.

Cohen, J.K., and J.W. Stockwell (1994). The SU User's Manual. Colorado School of Mines and Gas Research Institute, Chicago, Illinois.

Del Pezzo, E., F. Bianco and G. Saccorotti, 2003. Seismic source dynamics at Vesuvius volcano, Italy, J. Volcanol. Geoth. Res., 3017, 1-18.

De Luca, G., R. Scarpa, E. Del Pezzo and M. Simini (1997). Shallow structure of Mt. Vesuvius volcano, Italy, from seismic array analysis, Geophys. Res. Lett., 24, 481-484.

De Matteis, R., A. Zollo and J.P. Virieux (1997). P-wave arrival time inversion by using the tau-p method: application to the Mt. Vesuvius volcano, Southern Italy, Geophys. Res. Lett., 24, 515-518.

De Natale, G., P. Capuano, C. Troise and A. Zollo (1998). Seismicity at Somma-Vesuvius and its implications for the 3D tomography of the volcano, J. Volcanol. Geoth. Res., 82, 175-197.

De Natale, G., C. Troise, R. Trigila, D. Dolfi and C. Chiarabba (2004). Seismicity and 3D substructure at Somma-Vesuvius volcano: evidence for magma quencing, Earth Plan. Sci. Lett., 221, 181-196.

Di Maio, R., P. Mauriello, D. Patella, Z. Petrillo, S. Piscitelli, A. Siniscalchi and M. Veneruso (1997). Self-potential, geoelecrtic and magnetotelluric studies in Italian active volcanic areas, Annali di Geofisica, 40 (2), 519-537.

Di Stefano, R., and C. Chiarabba (2002). Active source tomography at Mt. Vesuvius: constraints for the magmatic system, J. Geophys. Res., 107 (B1), 2278; doi:10.1029/2001JB000792.

Ferrazzini, V., K. Aki and B. Chouet (1991). Characteristics of seismic waves composing Hawaiian volcanic tremor and gas-piston events observed by a near-source array, J. Geophys. Res., 96, 6199-6209.

Gasparini, P., and TomoVes Working Group (1998). Looking inside Mt.Vesuvius, Eos, Trans. Am. Geophys. Un., 79, 229-232.

Goldstein, P., and B. Chouet (1994). Array measurements and modeling of sources of shallow volcanic tremor at Kilauea Volcano, Hawaii, J. Geophys. Res., 99, 2637-2652.

Hakell, N.A. (1953). The dispersion of surface waves on multilayered media, Bull. Seismol. Soc. Am., 43, 1, 17-34.

Hansen, P.C. (1992). Analysis of discrete ill-posed problems by means of the L-curve, SIAM Rev., 34, 561-580.

Horike, M. (1985). Inversion of phase velocity of long-period microtremors to the S-wave-velocity structure down to the basement in urbanized areas, J. Phys. Earth, 33, 59-96.

Ibanez, J., E. Del Pezzo, J. Almendros, M. La Rocca, M. Alguacil, G. Ortiz and A. Garcia (2000). Seismo-volcanic signals at Deception Island volcano (Antartica): wavefield analysis and source modeling, J. Geophys. Res., 105, B6, 13905-13931.

Judenherc, S., and A. Zollo (2004). The bay of Naples (southern Italy): constraints on the volcanic structures inferred from a dense seismic survey, J. Geophys. Res., 109, B10312; doi:10.1029/2003JB002986.

La Rocca, M., E. Del Pezzo, M. Simini, R. Scarpa and G. De Luca (2001). Array analysis of seismograms from explosive sources: evidence for surface waves scattered at the main topographical features, Bull. Seismol. Soc. Am., 91, 219-231.

Lee, W.H.K., and D.A. Dodge, eds. (1992). A course on PC-based seismic networks, U.S.Geol.Survey Open-File Report, 92-441.

Lomax, A., A. Zollo, P. Capuano and J. Virieux (2001). Precise, absolute earthquake location under Somma Vesuvius volcano using a new three dimensional velocity model, Geophys. J. Int., 146, 313-331.

Metaxian, J.P., P. Lesage and J. Dorel (1997). Permanent tremor at Masaya volcano, Nicaragua: wave field analysis and source location, J .Geophys. Res., 102, 22529-22545.

Natale, M., C. Nunziata and G.F. Panza (2005). Average shear wave velocity models of the crustal striucture at Mt. Vesuvius, Phys. Earth. Plan. Int., 152, 7-21.

O'Connel, R., and B. Budianski (1977). Visco-elastic properties of fluid-saturated cracked solids, J. Geophys. Res., 82, 5719-5736.

Okabe, M. (1979). Analytical expressions for gravity anomalies due to homogeneous polyhedral bodies and translations into magnetic anomalies, Geophysics, 44, 730-741.

Okubo, P.G., H.M. Benz and B.A. Chouet (1997). Imaging the crustal magma sources beneath Mauna Loa and Kilauea volcanoes, Hawaii, Geology, 25, 867-870.

Patanè, D., C. Chiarabba, O. Cocina, P. De Gori, M. Moretti and E. Boschi (2002). Tomographic images and 3D earthquake locations of the seismic swarm precedine the 2001 Mt. Etna eruption: evidence for a dyke intrusion, Geophys. Res. Lett., 29; doi: 10.1029/2001GL014391.

Piana Agostinetti, N., and C. Chiarabba (2008). Seismic structure beneath Mt. Vesuvius from receiver func-

tion analysis and local earthquakes tomography: evidences for location and geometry of the magma chamber, Geophys. J. Int., 175, 1298-1302; doi:10.1111/j.1365-246X.2008.03868.x

Principe, C., M. Rosi, R. Santacroce and A. Sbrana (1987). Explanatory notes to the geological map, In: R. Santacroce (ed.), Somma-Vesuvius, Quaderni de "La Ricerca Scientifica", CNR, 114, 11-51.

Rosi, M., R. Santacroce and M.F. Sheridan (1987).Volcanic hazard, In: R. Santacroce (ed.), Somma-Vesuvius, Quaderni de "La Ricerca Scientifica", CNR, 114, 197-234.

Saccorotti, G., R. Maresca and E. Del Pezzo (2001). Array analyses of seismic noise at Mt. Vesuvius Volcano, Italy, J. Volcanol. Geotherm. Res.,110, 79-1006.

Saccorotti, G., G. Ventura and G. Vilardo (2002). Seismic swarms related to diffusive processes: the case of Somma-Vesuvius volcano, Italy, Geophysics, 67, 199-203.

Scarpa, R., F. Tronca, F. Bianco and E. Del Pezzo (2002). High resolution velocity structure beneath Mount Vesuvius from seismic array data, Geophys. Res. Lett., 29 (21), 2040; doi:10.1029/2002GL0155576.

Sheridan, M.F., F. Barberi, M. Rosi and R. Santacroce (1981). A model for Plinian eruptions of Vesuvius, Nature, 289, 282-285.

Stabile, T.A., A. Zollo, M. Vassallo and G. Iannaccone (2007). Underwater acoustic channel properties in the Gulf of Naples and their effects on digital data transmission, Annals of Geophysics, 50 (3), 411-426.

Tondi, R., and R. De Franco (2003). Three-dimensional modeling of Mount Vesuvius with sequential integrated inversion, J. Geophys. Res., 108 (B5), 2256; doi:10.1029/2001JB001578.

Tribalto, G., and A. Maino (1962). Rilevamento gravimetrico della zona circumvesuviana, Annali dell'Osservatorio Vesuviano, 4, 134-172.

Ventura, G., and G. Vilardo (1999). Seismic based estimate of hydraulic parameters at Vesuvius volcano, Geophys. Res. Lett., 26, 887-890.

Villasenor, A., H.M. Benz, L. Filippi, G. De Luca, R. Scarpa, G. Patanè and S. Vinciguerra (1998). Three-dimensional P-wave velocità structure of Mt.Etna, Italy, Geophys. Res. Lett., 25, 1975-1979.

Zhdanov, M.S. (2002). Geophysical inverse theory and regularization problems, Elsevier, Amsterdam, 628 pp.

Zollo, A., P. Gasparini, J. Virieux, H. Le Meur, G. De Natale, G. Biella, E. Boschi, P. Capuano, R. De Franco, P. Dell'Aversana, R. De Matteis, I. Guerra, G. Iannaccone, L. Mirabile and G. Vilardo (1996). Seismic evidence for a low-velocity zone in the upper crust beneath Mount Vesuvius, Science, 274, 592-594.

Zollo, A., W. Marzocchi, P. Capuano, A. Lomax and G. Iannaccone (2002). Space and time behaviour of seismic activity at Mt. Vesuvius volcano, Southern Italy, Bull. Seismol. Soc. Am., 92, 625-640.

*Corresponding author: Paolo Capuano,
Università di Salerno, Dipartimento di Fisica "E. R. Caianiello", Fisciano (Salerno), Italy; email: pcapuano@unisa.it.